

Received 4 February 2023, accepted 21 February 2023, date of publication 27 February 2023, date of current version 3 March 2023.

Digital Object Identifier 10.1109/ACCESS.2023.3249744

RESEARCH ARTICLE

Capacity Analysis and Data Detection of OvTDM-MIMO System

YUE HU 

Key Laboratory of Universal Wireless Communications, Ministry of Education, Beijing University of Posts and Telecommunications, Beijing 100876, China
School of Information and Communication Engineering, Beijing University of Posts and Telecommunications, Beijing 100876, China


e-mail: huyue2017@bupt.edu.cn

ABSTRACT It is well known that the channel capacity of traditional MIMO systems is positively correlated with the number of antennas, so MIMO systems usually use more antennas to meet higher system capacity requirements, which is increasingly conflicting with the miniaturization requirements of portable devices. To overcome the above problems, a new OvTDM-MIMO system is proposed, which can effectively improve the capacity of the system. This system introduces the overlapped time division multiplexing (OvTDM) technology into the MIMO system, which can further improve the channel capacity of the MIMO system by using a smaller number of antennas. This paper introduces the transceiver model of the OvTDM-MIMO system in detail and derives the channel capacity of the system based on mutual information theory. Compared with a conventional MIMO system, the OvTDM-MIMO system has the ability to improve channel capacity. Then, this paper proposes an OvTDM-MIMO symbol detection scheme based on an improved low-complexity Orthogonal Approximate Message Passing (OAMP) algorithm to solve the symbol detection problem caused by symbol correlation. The main design idea of this scheme is to use symbol correlation as the detection constraint and realizes joint symbol detection by combining adjacent symbols, avoiding the problem of excessive matrix size caused by Kronecker product operation. The simulation results show that the proposed detection algorithm can achieve similar performance to traditional MIMO system detection algorithms with low computational complexity.

INDEX TERMS Overlapped time division multiplexing, MIMO, channel capacity, detection scheme.

I. INTRODUCTION

To meet the diverse requirements of application scenarios and communication services, the data traffic of existing communication networks is growing rapidly [1], [2], [3]. The required data rate will rapidly exceed the capacity of the existing communication network in the near future. Since MIMO systems can achieve higher data rates through spatial multiplexing, they are widely used in modern communication systems. To meet the requirements of today's rapid data service development, the number of antennas required for MIMO systems is increasing, which contradicts the current demand for high-speed and miniaturization of portable devices. In view of the above problems, new technologies reduce the number and size of antennas are urgently needed

The associate editor coordinating the review of this manuscript and approving it for publication was Zesong Fei .

to increase the transmission rate of MIMO systems and meet the development goals of future communication networks.

To solve the above problems, a non-orthogonal transmission scheme is introduced into the MIMO system. Among them, various non-orthogonal transmission schemes (Faster-Than-Nyquist signaling (FTN) [4], [5], Spectrally Efficient Frequency Division Multiplexing (SEFDM) [6], [7], and Overlapped X Domain Multiplexing (OvXDM) [8], [9]) have effectively improved channel capacity by breaking through the limitations of the orthogonal modulation transmission systems. Taking overlapped time division multiplexing (OvTDM) technology as an example, it can transmit at rates faster than the Nyquist rate. For channels with limited bandwidth, it has the potential to increase the channel capacity. Furthermore, MIMO technology is widely employed in 4G and 5G standard protocols [10]. Combining MIMO technology with various non-orthogonal transmission

technologies, non-orthogonal transmission schemes can significantly improve the system channel capacity with a small antenna size.

This paper proposes an OvTDM-MIMO system architecture that combines OvTDM technology with MIMO system. The capacity of the OvTDM-MIMO system is derived, and the channel capacity of the OvTDM-MIMO system is proved to be equivalent to that of the FTN-MIMO system [11], [12], [13], [14]. It is worth noting that the overlap between symbols in the OvTDM-MIMO system destroys the orthogonality of symbols, which makes its signal detection very difficult. Because of the overlapping between symbols, the equivalent matrix of the OvTDM-MIMO system is too large, which poses a challenge to the low-complexity signal detection scheme. Traditional low-complexity detection algorithms (Fano algorithm [15], MSJD algorithm [16], etc.) are usually used for the detection of OvXDM signals in SISO systems, and cannot be directly applied to OvTDM-MIMO systems. The expected propagation (EP) algorithm [17], [18] has the advantages of low complexity and good detection performance in MIMO signal detection. The eigenvalue distribution of the equivalent matrix of the OvTDM-MIMO system is far from that of the Gaussian matrix, so the performance of the EP algorithm cannot be guaranteed to be optimal. Therefore, developing a new low-complexity signal detection scheme is the focus of this paper. Therefore, a multi-symbol joint detection scheme is proposed to overcome the high complexity signal detection problem caused by symbol correlation. This detection scheme uses the constraint relationship between symbols as the decoding constraint, and uses the orthogonal approximate message passing (OAMP) algorithm [19], [20] which is robust to the correlation between symbols to detect the received signals. Simultaneously, the detection scheme adopts the conjugate gradient (CG) method [21] to simplify the algorithm iteration process, thereby reducing the complexity of the OAMP iteration process. The simulation results show that the proposed detection scheme can achieve good detection performance with low-computational complexity.

The main contributions of this paper are as follows:

- 1) The OvTDM-MIMO system architecture has been proposed and demonstrated to have the potential to increase channel capacity compared to conventional MIMO systems, achieving a trade-off between higher channel capacity and a smaller number of antennas.
- 2) A symbol detection scheme based on improved low complexity orthogonal approximate message passing (OAMP) is proposed for the OvTDM-MIMO system. The scheme uses symbol correlation as the detection constraint, and realizes joint symbol detection by combining adjacent symbols, which avoids the problem of large matrix scale caused by Kronecker product operation and reduces the computational complexity.

The remainder of this article is structured as follows:

Section II describes the model and signal characteristics of the OvTDM-MIMO system. Section III uses

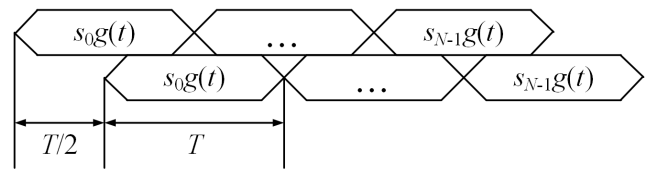


FIGURE 1. The OvTDM symbols generation process.

information theory to calculate the channel capacity of the OvTDM-MIMO system. Section IV provides a multi-symbol joint detection strategy and analyzes the performance of the proposed algorithm. The simulation results are discussed in Section V and summarized in Section VI.

II. SYSTEM MODEL

A. OvTDM SYSTEM MODEL

A continuous time domain OvTDM signal is given by Eq. (1).

$$x(t) = \frac{1}{\sqrt{K}} \sum_{n=0}^{N-1} s_n g(t - nT/K), \quad (1)$$

where s_n denotes the modulation symbols to be transmitted. The modulation symbol length and waveform symbol period are represented by N and T , respectively. K is an overlapped multiplexing coefficient representing the degree of symbol overlap. The energy normalization operation is $1/\sqrt{K}$.

Figure 1 shows the generation process of OvTDM symbols. This process generates OvTDM symbols by shifting and weighting multistream time-limiting symbols. Where the output waveform of the reshaping filter is the energy normalized real waveform $g(t)$, which satisfies

$$\int_{-T/2}^{T/2} |g(t)|^2 dt = \int_{-B/2}^{B/2} |G(f)|^2 df = 1, \quad (2)$$

In theory, there is no waveform that is both rigorously time-limited and band-limited. The bandwidth of $g(t)$ is considered to be $B/2$, which means that the energy of its power spectral function $|G(f)|^2$ is largely concentrated in the $[-B/2, B/2]$ region.

After passing through the additive white Gaussian noise channel, the received waveform signal $r(t)$ is expressed as

$$r(t) = \frac{1}{\sqrt{K}} \sum_{n=0}^{N-1} s_n g(t - nT/K) + w(t), \quad (3)$$

where $w(t)$ represents additive white Gaussian noise (AWGN).

The quadrature receiver is used to process the received signal $r(t)$. Then the output symbol $y(t)$ is

$$y(t) = r(t) p(mT/K - t), \quad (4)$$

where $p(t)$ is the pulse response of the receiver filter, which is a rectangular pulse at an interval of $[0, T/K)$ with energy-normalized pulse. The receiver samples once every T/K

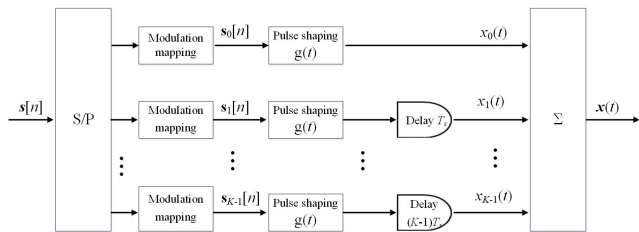


FIGURE 2. The schematic diagram of the transmitter of the OvTDM system.

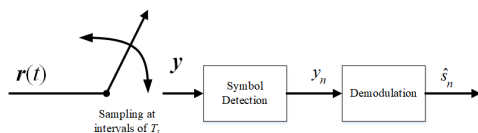


FIGURE 3. The schematic diagram of the receiver of the OvTDM system.

seconds and its corresponding discrete time domain signal is expressed as

$$y_m = y\left(\frac{mT}{K}\right) = \frac{1}{\sqrt{K}} \sum_{k=0}^{K-1} s_{m-k} g\left(t - \frac{kT}{K}\right) p\left(\frac{mT}{K} - t\right). \quad (5)$$

where $w_m = \int_{(m-1)T/K}^{mT/K} w(t) p(t - mT/K) dt$ denotes the noise sequence. This formula shows that the received signal includes not only the desired signal at the corresponding time but also the adjacent $K - 1$ signals. This makes it no longer satisfies the independence property between symbols, which poses a challenge for signal detection.

Figure 2 and Figure 3 show the schematic diagrams of the transmitter and receiver of the OvTDM system, respectively.

B. OvTDM-MIMO SYSTEM MODEL

Figure 4 depicts an OvTDM-MIMO ($K = 2; 2 \times 2$) system. Where N_T and N_R are the numbers of antennas of the transmitter and receiver respectively. The main difference between this system and the traditional MIMO system is that the overlap between symbols is introduced at the transmitter.

1) OvTDM-MIMO SYSTEM MODEL

The $i \in \{0, 1, \dots, N_T - 1\}$ -th transmit antenna's transmit signal is

$$x_i(t) = \sum_{n=0}^{N-1} \frac{1}{\sqrt{N_T K}} s_{i,n} g(t - nT/K), \quad (6)$$

where $g(t)$ represents the energy-normalized modulation pulse and $s_{i,n}$ represents the n -th transmit symbol from the i -th transmit antenna.

Through MIMO channel, the receiving waveform at $j \in \{0, 1, \dots, N_R - 1\}$ of each receiving antenna is shown as

$$r_j(t) = \sum_{i=0}^{N_T-1} \sum_{n=0}^{N-1} \frac{1}{\sqrt{N_T K}} h_{j,i} s_{i,n} g(t - nT/K) + w_i(t), \quad (7)$$

where $h_{j,i}$ denotes the path gain between the i -th transmit and j -th receive antennas, and $w_i(t)$ denotes the AWGN influencing the received signal at antenna j .

Figure 4 shows the OvTDM-MIMO ($K = 2, 2 \times 2$) system architecture. The continuous-time waveform $j \in \{0, 1, \dots, N_R - 1\}$ at the receive antenna $y_j(t)$ is

$$y_j(t) = r_j(t) p(mT/K - t). \quad (8)$$

Figure 5 describes the sampling example of the receiver. Figure 5 clearly shows that each sampled signal intentionally overlaps the transmission waveform. At time $m (0 \leq m \leq N + K - 2)$, the output $y_j[m]$ is

$$y_j[m] = \sum_{i=0}^{N_T-1} \sum_{n=0}^{N-1} \frac{1}{\sqrt{N_T K}} h_{j,i} s_{i,n} g(t - nT/K) \cdot p(mT/K - t) + w_i(t) p(mT/K - t). \quad (9)$$

Compared with traditional MIMO systems, the signal flow generated by OvTDM-MIMO systems will generate $K - 1$ additional samples. This is different from traditional MIMO systems.

2) DISCRETE TIME CHANNEL MODEL

To better describe the model of the OvTDM-MIMO system, it describes the signal-generating process of the OvTDM-MIMO system in matrix form.

Assuming that there is a separate overlap relationship between the OvTDM signals, the matrix \mathbf{G} is given by the following formula.

$$\mathbf{G} = \begin{pmatrix} g_0 & 0 & \cdots & 0 \\ \vdots & g_0 & & \vdots \\ g_{K-1} & \vdots & \ddots & 0 \\ 0 & g_{K-1} & & 0 \\ 0 & 0 & \ddots & g_0 \\ \vdots & \vdots & & \vdots \\ 0 & 0 & \cdots & g_{K-1} \end{pmatrix}, \quad (10)$$

where g_i denotes the correlation of the i -th received waveform pulse with the receiver's basis function $p(t)$.

Then, the OvTDM-MIMO system channel matrix is equivalent to

$$\mathbf{H}_{Eq} = \begin{pmatrix} h_{0,0} \mathbf{G} & \cdots & h_{0,N_T-1} \mathbf{G} \\ \vdots & \ddots & \vdots \\ h_{N_R-1,0} \mathbf{G} & \cdots & h_{N_R-1,N_T-1} \mathbf{G} \end{pmatrix} = \mathbf{H} \otimes \mathbf{G}, \quad (11)$$

where \mathbf{H} represents the matrix of the MIMO channel and \otimes represents the operation of Kronecker product.

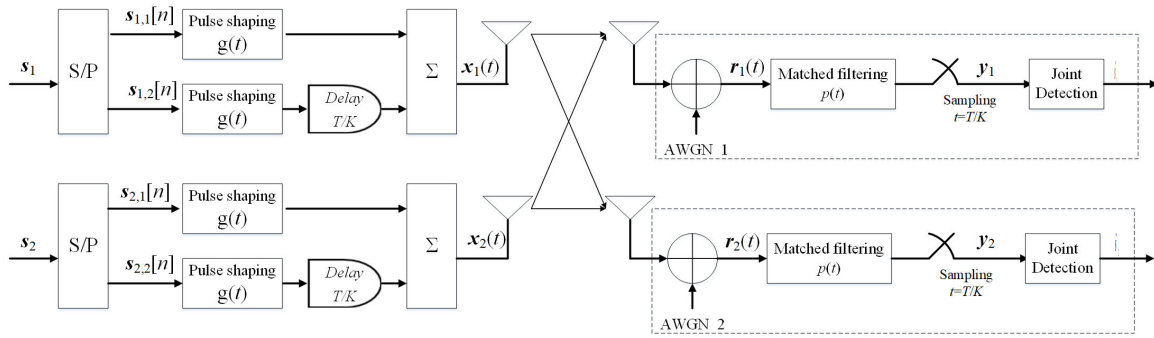


FIGURE 4. The orthogonalized receiver architecture for OvTDM-MIMO ($K = 2, 2 \times 2$).

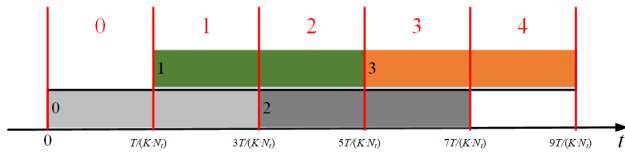


FIGURE 5. The sampling example for OvTDM-MIMO system.

Then the OvTDM-MIMO system is rewritten as

$$y = H_{Eq}s + w, \tag{12}$$

It is assumed that the noise from different antennas is uncorrelated. Because each received sample is completely independent of the adjacent samples in the previous section, the noise is completely uncorrelated. Q_w is the noise covariance matrix. It has

$$Q_w = \sigma^2 I_{N_R(N+K-1)}. \tag{13}$$

where w denotes the noise matrix corresponding to the MIMO channel and σ^2 the variance of Gaussian white noise.

III. CHANNEL CAPACITY

The channel capacity is defined as the maximum value of mutual information, that is,

$$C = \mathbb{E} \left(\lim_{N \rightarrow \infty} \max_{p_s(s)} \frac{1}{KN + K - 1} I(s; y) \right), \tag{14}$$

where $I(s; y)$ represents the system's mutual information. s is a Gaussian random vector with covariance Q_s , where Q_s is the covariance of the transmitted bits. The maximum value of mutual information has been established.

$$I(s; y) = H(y) - H(w), \tag{15}$$

where $H(y)$ represents the differential entropy of y , and $H(w)$ represents the differential entropy of w .

Since the transmitted data and noise are assumed to be independent, $H(y)$ has

$$H(y) = \log_2 \det \left(H_{Eq} Q_s H_{Eq}^H + Q_w \right), \tag{16}$$

$H(w)$ has

$$H(w) = \log_2 \det(Q_w), \tag{17}$$

Therefore, combining Eq.(16) and Eq.(17), Eq.(15) is transformed into

$$I(x; y) = \log_2 \frac{\det \left(H_{Eq} Q_s H_{Eq}^H + Q_w \right)}{\det(Q_w)}. \tag{18}$$

Then the channel capacity is expressed as:

$$C = \frac{1}{NT + (K - 1) T/K} \cdot \log_2 \det \left(I_{N_R(N+K-1)} + \frac{H_{Eq} Q_s H_{Eq}^H}{\sigma^2} \right). \tag{19}$$

To better demonstrate the channel capacity potential of the OvTDM-MIMO system, it is compared with the FTN-MIMO system and the traditional MIMO system. The channel capacity curves of the three MIMO systems are shown in Figure 6. Figure 6 shows that the channel capacities of the OvTDM-MIMO system and the FTN-MIMO system are similar under the same number of antennas. For the same number of antennas, the channel capacity of the OvTDM-MIMO system is significantly larger than that of the MIMO system. This shows that the OvTDM-MIMO systems can achieve higher channel capacity with fewer antennas at the cost of higher inter-symbol correlation. Because the introduction of symbol overlap destroys the orthogonality between symbols, it will be difficult for symbol detection.

IV. DETECTION ALGORITHM

A. ML DETECTION

The correlation between symbols makes symbol detection complex in OvTDM-MIMO systems. For such systems, the maximum likelihood (ML) algorithm is usually used as the optimal detection algorithm. Its detector is

$$\hat{s} = \arg \min_{s \in \Omega} \|\hat{y} - H_{Eq}s\|^2. \tag{20}$$

where Ω represents the constellation set of all transmitted symbols.

As shown in the previous sections, the equivalent matrix H_{Eq} is generated by the Kronecker product of the waveform correlation matrix G between OvTDM symbols and the MIMO channel matrix H , and its matrix size is very large.

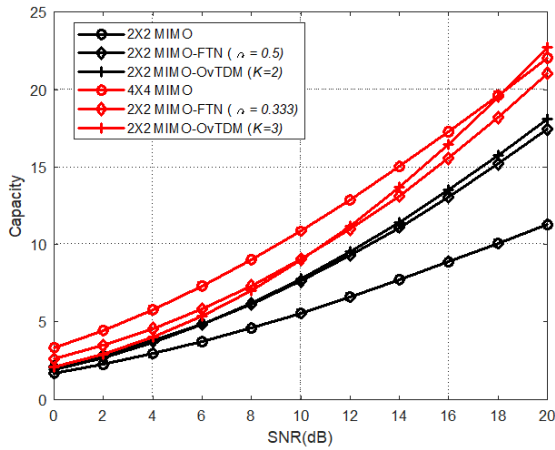


FIGURE 6. The comparison of channel capacities for different systems.

If the ML algorithm is used for signal detection, it will lead to very high computational complexity, making it difficult to apply this algorithm in practical projects. If low-complexity ZF and MMSE detection algorithms are used for signal detection, the correlation between OvTDM symbols severely limits the performance of ZF and MMSE detection algorithms. Therefore, developing a low-complexity detection algorithm is a key component of OvTDM-MIMO signal detection.

B. A TWO STAGE JOINT DETECTION

To simplify the signal detection process, a two-level joint detection scheme is proposed in this paper. The main idea of this scheme is to divide the signal detection process into two parts: channel equalization and OvTDM symbol detection. This method reduces the computational complexity of the detection algorithm by reducing the size of the equivalent matrix H_{Eq} .

The signal detection process is as follows:

$$\hat{x} = \arg \min \|\hat{y} - Hx\|^2, \quad (21)$$

$$\hat{s} = \arg \min_{s \in \Omega} \|\hat{x} - Gs\|^2. \quad (22)$$

In the first stage, the algorithm mainly adopts the ZF criterion or the MMSE criterion to perform MIMO channel equalization on the received signal and obtain the OvTDM sequence. In the second stage, the estimated transmission signal is obtained by performing OvTDM signal detection on the equalized signal sequence.

This method avoids the large-scale matrix operation caused by the direct calculation of the Kronecker product. The types of algorithms used in the two stages can be flexibly adjusted according to actual needs. Simultaneously, considering the coding characteristics of OvTDM symbols, the expected propagation (EP) algorithm [17], [18] can be used for OvTDM symbol detection, which effectively improves the performance of OvTDM symbol detection. This paper proposes an MMSE-EP algorithm, and its pseudocode is shown in Algorithm 1.

Algorithm 1 A MMSE-EP Algorithm

Input: $y, N_t, N_r, I_{EP}, N, K, H, SNR$

Output: \hat{s}

```

1: function EP ( $y, N, I_{EP}, K, H, SNR$ )
2:   Initialization parameters,
3:   combining  $K$  and  $H$  to construct Matrix  $\hat{H}$ ,
4:   for  $n = 1 : N$  then
5:     initialise  $\gamma, \Gamma, cav_i$ ,
6:     Set the mean and variance vectors of all marginal
7:      $q_i(x)$  during iteration,
8:     for  $l = 1 : I_{EP}$  then,
9:       calculate Mean ( $t_i$ ) and variance ( $h_i^2$ ) of each
10:      cavity marginal
11:      Compute cavity marginal for each  $x_i$ ,
12:      Normalize distribution
13:      Mean ( $v_{p_i}$ ) and variance ( $var_{p_i}$ ) of distribution,
14:      Compute new values for  $\gamma$  and  $\Gamma$ ,
15:      meand and variance vectors of all marginal
16:       $q_i(x)$  at next,
17:    end for
18:  approximate values  $\hat{x}$  are obtained,
19: end for
20: Demodulate  $\hat{x}$ , and to get  $\hat{s}$ ,
21: return  $\hat{s}$ .
22: end function

23: function MAIN
24:   Initialize  $\hat{s}$ 
25:   for  $n = 1 : N$  then
26:      $H_{MMSE} = inv((H_n^H H_n) + \sigma^2 I) H_n y_n$ ;
27:     Select  $y_n$  and  $H_n$ ;
28:      $\hat{s}_n = functionEP(y_n, N_t, I_{EP}, K, H_n, SNR)$ ;
29:   end for
30: return  $\hat{s}$ .

```

Because the correlation between OvTDM symbols amplifies the impact of noise, the symbol sequence obtained after MIMO channel equalization is seriously distorted, which affects the subsequent OvTDM signal detection. Therefore, this algorithm must be improved to improve the system performance.

C. IMPROVED OAMP ALGORITHM

Aiming at the above problems, a signal detection algorithm based on improved OAMP is proposed, according to the characteristics of the OvTDM MIMO system. This algorithm takes advantage of the characteristic that the same symbol information will be extended to adjacent $K - 1$ OvTDM symbols and introduces the idea of serial iterative elimination to offset the influence of symbol correlation. The proposed detection algorithm ensures the decoding performance while reducing the complexity of the decoding code.

Assuming that multiple OvTDM symbols in an OvTDM system contain the same waveform symbol, an iterative detection method can further improve signal detection

performance. The iterative process of signal detection is as follows:

$$\hat{y}_n = y_n - \sum_{k=1}^{K-1} h_{n-k} g_{K-k} s_{n-k}, \quad n = 0, 1, \dots, KN - 1. \quad (23)$$

This operation ensures that the decoding result does not interfere with the subsequent decoding process. The detection performance of the proposed detection algorithm can be further improved.

If the previous judgment output of the detected symbol is correct, the previous formula is rewritten as

$$\hat{y}_n = h_n g_0 s_n + w_n, \quad (24)$$

The signal detection problem is now reduced to a quasi-MIMO signal detection problem. OAMP algorithm can overcome the influence of inter-symbol correlation, so an improved OAMP signal detection method is proposed to solve this problem.

The iteration formula of OAMP is expressed as [13], [14]

$$r^t = \hat{s}^t + W_t (y_n - h_n g_0 \hat{s}^t), \quad (25)$$

$$s^{t+1} = \eta_t (r^t). \quad (26)$$

where W_t is the decorrelation matrix, η_t is the divergence-free constraint, and t is the current number of iterations.

The difference between the nonlinear estimation result s^t and the actual value is q^t , and the difference between the linear estimation result r^t and the real value is h^t , and their values are shown as follows

$$h^t = B_t q^t + W_t n, \quad (27)$$

$$q^{t+1} = \eta_t (s + h^t) - s. \quad (28)$$

The corresponding OAMP state evolution are

$$v_t^2 = \frac{(y - h_n g_0 \hat{s}^t)^H (y - h_n g_0 \hat{s}^t - I * \sigma^2)}{\text{tr}((h_n g_0)^H (h_n g_0))}. \quad (29)$$

$$\tau_t^2 = \frac{\text{tr}(B_t * B_t^H) * v_t^2}{N} + \frac{\text{tr}(W_t * \sigma^2 * I_{N+K-1} * W_t^H)}{N}. \quad (30)$$

where v_t^2 and τ_t^2 represent nonlinear mean square error and linear mean square error, respectively.

It is assumed that the transmitted bit information satisfies the i.i.d condition and is independent of the additive white Gaussian noise. The estimation expression of nonlinear mean square error v_t^2 is

$$\tau_t^2 = \frac{(y - (h_n g_0) \hat{s}^t)^H (y - (h_n g_0) \hat{s}^t - I * \sigma^2)}{\text{tr}(((h_n g_0))^H ((h_n g_0)))} \xrightarrow{N \rightarrow \infty} 1. \quad (31)$$

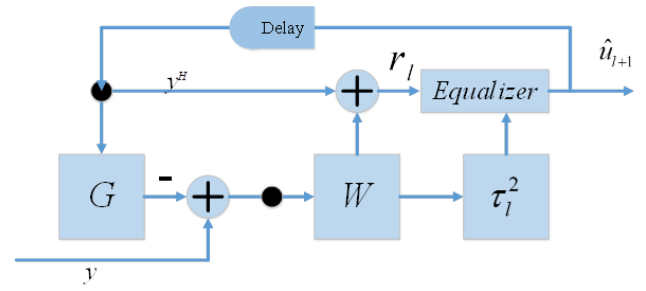


FIGURE 7. The schematic diagram of improved OAMP detector.

This shows that the nonlinear mean square error is approximated to a fixed value when the constellation modulation satisfies the probability distribution and the transmission signal satisfies the i.i.d condition.

There is a linear estimate r^t .

$$\begin{aligned} r^t &= \hat{s}^t + W_t (y_n - (h_n g_0) \hat{s}^t) \\ &= \hat{s}^t + \frac{N}{\text{tr}(\hat{W}_t (h_n g_0))} \hat{W}_t (y_n - (h_n g_0) \hat{s}^t) \\ &= \hat{s}^t + \frac{N}{\text{tr}(\hat{W}_t (h_n g_0))} (h_n g_0) \\ &\quad \cdot \left((h_n g_0) (h_n g_0)^T + \frac{\sigma_w^2}{I} \right)^{-1} \\ &\quad \cdot (y_n - (h_n g_0) \hat{s}^t). \end{aligned} \quad (32)$$

The calculation process for linear estimation r^t includes matrix inversion, matrix transposition, and other operations. The conjugate gradient (CG) algorithm replaces the complex matrix operation steps in solving the approximate solution of the linear equation.

Define A and B as

$$A = \left((h_n g_0) (h_n g_0)^T + \frac{\sigma_w^2}{I} \right), \quad (33)$$

$$B = (y_n - (h_n g_0) \hat{s}^t). \quad (34)$$

Let the matrix $AX = B$ solve the linear equation X . The linear system is then solved using the CG algorithm. Merging Eqs. (33) and (34) into Eq. (32), and the updated results are as follows.

$$r^t = \hat{s}^t + \frac{N}{\text{tr}(\hat{W}_t (h_n g_0))} (h_n g_0) X. \quad (35)$$

In order to prove the convergence of the proposed algorithm, this paper analyzes the AMP algorithm, the OAMP algorithm, and the proposed algorithm. See the appendix for the proof process.

This section proposes an improved OAMP signal detection scheme based on the above design. Figure 7 depicts the detector structure. Algorithm 2 describes the process of the proposed decoder.

Algorithm 2 The Proposed Detection Algorithm**Input:** $y, N_t, N_r, I_{OAMP}, I_{CG}, N, K, \mathbf{H}, SNR$ **Output:** \hat{s}

```

1: function CG ( $y, K, I_{CG}, \mathbf{H}$ ),
2:   Initialize  $x, r$  and  $\eta$ ,
3:   Combine  $K$  and  $\mathbf{H}$ , obtain  $\hat{\mathbf{H}}$ ,
4:   while  $\sqrt{r^H r} > \eta$  &&  $i < I_{CG}$ 
5:      $i = i + 1$ ,
6:     if  $i == 1$ 
7:        $p_t = r_t$ ,
8:     else
9:        $\beta = r_t^H * r_t / (r_{t-1}^H * r_{t-1})$ ,
10:       $p_t = r_t + \beta * p_t$ ,
11:    end if
12:     $\alpha = r_t^H * r_t / (p_t^H * \hat{\mathbf{H}} * p_t)$ ,
13:     $x_t = x_t + \alpha * p_t$ ,
14:     $r_{t-1} = r_t$ ,
15:     $r_t = r_t - \alpha * \hat{\mathbf{H}} * x_t$ ,
16:  end while

17: function OAMP ( $y, N, I_{OAMP}, K, \mathbf{H}, SNR$ ),
18:   Initialize  $\tau_t^2$  and  $x_t$ ,
19:   for  $n = 1 : I_{OAMP}$  then
20:     Compute  $v_t^2, \hat{W}_t$  and  $W_t$ ,
21:     Compute  $r_t = \text{function CG}(y, K, I_{CG}, \mathbf{H})$ ,
22:     if  $k \geq 2$  then
23:       Compute  $B_t$  and  $\tau_t^2$ ,
24:     end if
25:     for  $n = 1 : N$  then
26:       Initialization parameters  $temp1$  and  $temp2$ ,
27:       for  $m = 1 : M$  then
28:          $\hat{s} = \mathbb{E} \{s|r^t, \tau^t, M\}$ 
29:       end for
30:     end for
31:   end for
32: return  $\hat{s}$ .
33: end function

34: function MAIN
35:   Initialize  $\hat{s}$ 
36:   for  $n = 1 : N$  then
37:     Select  $y_n$  and  $\mathbf{H}_n$ ;
38:     Combining the known  $\hat{s}_n$  and  $y_n$ , obtain  $\hat{y}_n$ ;
39:    $\hat{s}_n = \text{function OAMP}(\hat{y}_n, N_t, I_{OAMP}, K, \mathbf{H}_n, SNR)$ ,
40:   end for
41: return  $\hat{s}$ .

```

D. COMPLEXITY ANALYSIS

The computational complexity of the improved OAMP algorithm is examined in this section.

The computational complexity of the proposed algorithm is compared to that of other algorithms in Table 1. Table 1 shows that the proposed algorithm has a significantly lower computational complexity than OAMP.

TABLE 1. The complexity comparison between the proposed algorithm and other algorithms.

Scheme	Complexity
MMSE-Viterbi	$\mathcal{O}(N \cdot (N_t)^3 + KN \cdot 2^{K+1})$
MMSE-EP	$\mathcal{O}(N \cdot (N_t)^3 + I_{EP} \cdot (KN)^3)$
MMSE-OAMP	$\mathcal{O}(N \cdot (N_t)^3 + I_{OAMP} \cdot ((KN)^3/3 + 3(KN)^2))$
Proposed algorithm	$\mathcal{O}(N \cdot (N_t)^3 + KN \cdot I_{OAMP} \cdot (I_{CG} \cdot N_t^2 + 3 \cdot (N_t)^2))$

TABLE 2. Simulation parameters.

Parameter	Value
Modulation	BPSK
Channel Type	Rayleigh fading channel
Overlapping multiplexing coefficient K	2, 3, 5
The number of iterations of EP	10
The number of iterations of OAMP	10
The number of iterations of CG	10
Multiplex waveform	Rectangular wave
The number of bits	10^5

Compared with traditional linear receivers, the complex multiplications of OAMP are affected by the number of iterations I_{OAMP} . If the cost of calculating the trajectory is ignored, the complexity of each iteration of OAMP is $\mathcal{O}(I_{OAMP} \cdot ((KN)^3/3 + 3(KN)^2))$, including direct matrix inversion and three matrix vector multiplication.

The proposed method uses the CG scheme for solving linear equations. Since the matrix inversion is replaced by CG solving linear equations, the computational complexity is $\mathcal{O}(N_t^2)$. With the influence of the number of iterations I_{CG} in the CG algorithm, the computational complexity of the entire algorithm is $\mathcal{O}(N \cdot (N_t)^3 + KN \cdot I_{OAMP} \cdot (I_{CG} \cdot N_t^2 + 3 \cdot (N_t)^2))$.

V. SIMULATION ANALYSIS

In this section, the performance of the proposed algorithm is simulated and analyzed. Table 2 shows the simulation parameters. It is assumed that MIMO channel coefficients \mathbf{H} remain constant within symbol blocks and change between symbol blocks.

The performance of the improved OAMP detection algorithm is compared to that of the MMSE-Viterbi detection algorithm and the MMSE-EP detection algorithm in this paper. Figure 8 depicts the simulation results. Figure 8 clearly shows that the MMSE-EP detection algorithm outperforms the MMSE-Viterbi detection algorithm. The reason

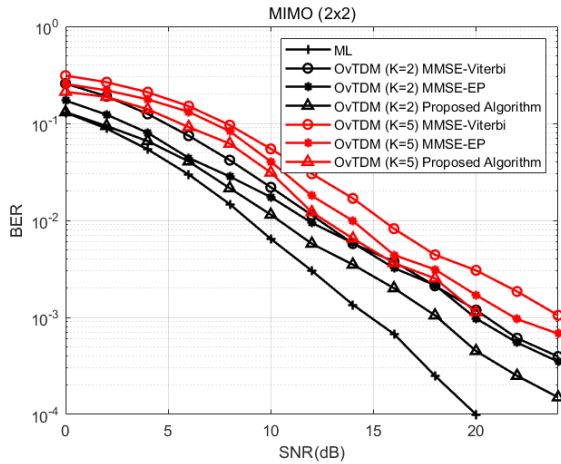


FIGURE 8. The comparison of different algorithms in OvTDM-MIMO (2 × 2) system.

for this is that the MMSE-Viterbi detection algorithm’s performance is poor because channel equalization amplifies the impact of noise. Through mean value and variance propagation, the MMSE-EP detection algorithm simplifies complex message delivery rules and has high robustness to noise effects amplified by channel equalization. Furthermore, the proposed improved OAMP detection algorithm outperforms the MMSE-EP detection algorithm. This is because the MMSE-EP detection algorithm suffers from severe error propagation problems due to channel equalization, while the proposed improved OAMP detection algorithm is based on the concept of serial interference cancellation and is more robust to the error propagation problem. Furthermore, the proposed OAMP-based detection algorithm outperforms ML algorithms for traditional MIMO. In terms of computational complexity, the proposed improved OAMP detection algorithm is most suitable for signal detection in OvTDM-MIMO systems.

This paper compares the system performance under different antenna numbers to further verify the performance of the proposed improved OAMP detection algorithm. The simulation results are shown in Figure 9. Figure 9 shows that the performance of the proposed improved OAMP detection algorithm is similar to that of the ML algorithm for MIMO systems with the same number of antennas. However, as the number of antennas increases, the detection performance gap between the two algorithms also increases. This is due to the fact that the proposed improved OAMP detection algorithm is limited by the estimated linear mean square error, and the error value increases as the antenna size increases. As a result, the above results were obtained.

This paper compares the detection performance under different modulation constellations, and the simulation results are shown in Figure 10. It can be seen from Figure 10 that the performance of the proposed detection algorithm decreases gradually with the increase of modulation order. This is because the increase of modulation order and symbol

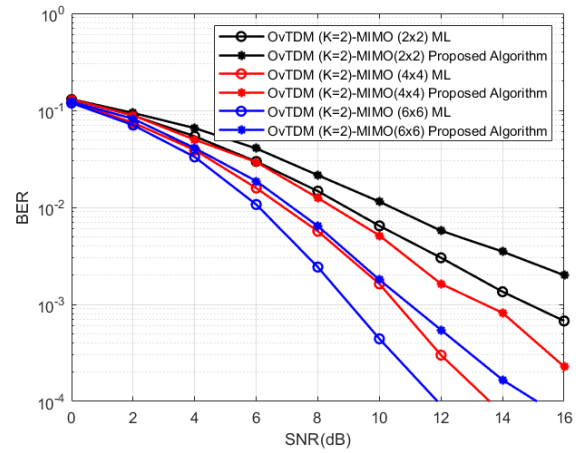


FIGURE 9. The comparison of algorithm performance in OvTDM-MIMO (K = 2) system with different antenna numbers.

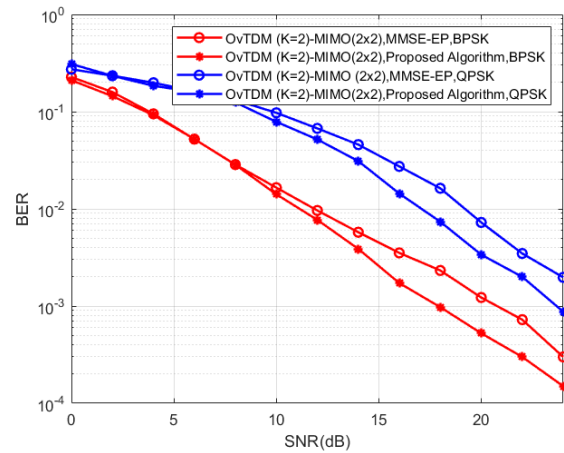


FIGURE 10. The performance comparison of different algorithms with different modulation constellations.

superposition jointly affect the received signal to show more waveform superposition states. However, various signal detection algorithms will have performance degradation in the face of this situation. Therefore, it is very important to select an appropriate modulation scheme according to different channel state information.

VI. CONCLUSION

This paper introduces the OvTDM technology into the MIMO system to further improve the system capacity. This paper proposes an OvTDM-MIMO system architecture, describes its discrete-time channel modes and derives its corresponding channel capacity. Simultaneously, it is demonstrated that it has the potential to increase the system capacity compared with traditional MIMO systems. But the correlation between symbols caused by symbol overlap leads to the problem of signal detection. To address the signal detection issue, an improved OAMP for OvTDM-MIMO signal detection is proposed. The concept exploits the fact that multiple symbols contain the same waveform symbol, and it uses

the OAMP algorithm to detect OvTDM symbols to improve detection performance. Then, the CG algorithm is used to approximate the solution of the linear equation to reduce the complexity of the iterative calculation in the OAMP algorithm. Simulation results show that the computational complexity of the proposed OvTDM signal detection scheme is much lower than that of the MMSE-Viterbi algorithm. The proposed OvTDM-MIMO system is suitable for special scenarios such as high capacity and limited number of antennas in the future, and provides useful technical ideas for the new generation of communication networks.

APPENDIX

A. THE PROOF OF AMP ALGORITHM'S CONVERGENCE

AMP problem model:

$$\mathbf{y} = \mathbf{A}\mathbf{x} + \mathbf{n}, \tag{36}$$

$$x_j \sim P_X(x), \quad \forall \mathbf{x}. \tag{37}$$

where $\mathbf{A} \in M \times N$ is the perception matrix, \mathbf{x} is a Gaussian vector with a mean of 0 and a variance of σ^2 .

Given the real \mathbf{x} , it can be based on the result of state evolution τ^t . Predict the mean square error (MSE) $\mathbb{E}[\|\mathbf{x} - \hat{\mathbf{x}}^t\|_2^2]$ between the estimated \mathbf{x}^t and the true value \mathbf{x} of AMP in the t iteration. It is expressed as

$$\tau_t^2 \rightarrow \frac{1}{N} \|\mathbf{x} - \hat{\mathbf{x}}^t\|_2^2, (N \rightarrow \infty). \tag{38}$$

\mathbf{q}^t is the difference between the nonlinear estimation result \mathbf{s}^t and the true value \mathbf{x} , and \mathbf{h}^t is the difference between the linear estimation result \mathbf{r}^t and the true value \mathbf{x} . They are respectively expressed as

$$\mathbf{q}^t = \mathbf{s}^t - \mathbf{x}, \tag{39}$$

$$\mathbf{h}^t = \mathbf{r}^t - \mathbf{x}. \tag{40}$$

where \mathbf{s}^t is the nonlinear estimation result, and \mathbf{r}^t is the linear estimation result.

The evolution corresponding to AMP is directly given by the following formula.

$$\tau_t^2 = \frac{N}{M} v_t^2 + \sigma^2, \tag{41}$$

$$v_{t+1}^2 = \{[\eta_t (X + \tau_t Z) - X]\}. \tag{42}$$

where v_t^2 is a nonlinear mean square error and τ_t^2 is a nonlinear estimation. η_t is a Lipschitz continuous function (component-wise) about \mathbf{r}^t .

The result model of each iteration is equivalent to

$$\hat{\mathbf{X}}^t = X + \tau_t^2 Z, Z \sim \mathcal{N}(0, 1), \tag{43}$$

$$\hat{\mathbf{X}}^t \sim \mathcal{N}(X, \tau_t^2). \tag{44}$$

τ_t^2 is approximated to $\hat{\tau}_t^2$, specifically expressed as

$$\tau_t^2 \approx \hat{\tau}_t^2 = \frac{1}{N} \|\mathbf{r}^t - \mathbf{s}^t\|_2^2. \tag{45}$$

Because the above formula is close to, not strictly equal to, because $\frac{1}{N} \|\mathbf{x} - \hat{\mathbf{x}}^t\|_2^2$ is about the second order Lipschitz

function of, which satisfies the following convergence relationship

$$\frac{1}{N} \|\mathbf{x} - \hat{\mathbf{x}}^t\|_2^2 \rightarrow \mathbb{E}[\|\mathbf{x} - \hat{\mathbf{x}}^t\|_2^2], (N \rightarrow \infty). \tag{46}$$

Only when \mathbf{A} is a Gaussian matrix or a sub-Gaussian matrix can the state evolution be consistent with the results of the AMP estimation. If the distribution of the eigenvalues of the perception matrix and the distribution of the eigenvalues of the Gaussian matrix are far different, the performance of the AMP cannot be guaranteed, and even may not converge.

B. THE PROOF OF OAMP ALGORITHM'S CONVERGENCE

Iterative formulas of OAMP are

$$\mathbf{r}^t = \mathbf{s}^t + \mathbf{W}_t (\mathbf{y} - \mathbf{A}\mathbf{s}^t), \tag{47}$$

$$\mathbf{s}^{t+1} = \eta_t(\mathbf{r}^t). \tag{48}$$

where $\mathbf{B}_t = \mathbf{I} - \mathbf{W}_t \mathbf{A}$, assuming

$$\tau_t^2 = \frac{1}{N} \mathbb{E}[\|\mathbf{h}^t\|_2^2], \tag{49}$$

$$v_{t+1}^2 = \frac{1}{N} \mathbb{E}[\|\mathbf{q}^{t+1}\|_2^2]. \tag{50}$$

In combination with OAMP iterative formula $\mathbf{r}^t = \mathbf{s}^t + \mathbf{W}_t (\mathbf{A}(\mathbf{x} - \mathbf{s}^t) + \mathbf{n})$, the parameter v^2 in LMMSE represents

$$[(\mathbf{x} - \mathbf{s}^t)(\mathbf{x} - \mathbf{s}^t)^T] = v^2 \mathbf{I}. \tag{51}$$

The two MSEs can be regarded as two parameters of the decorrelation matrix \mathbf{W}_t and the divergence-free function.

OAMP-state evolution is

$$\begin{aligned} \tau_t^2 &= \frac{1}{N} [\|\mathbf{h}^t\|_2^2] \\ &= \mathbb{E}[\text{tr}(\mathbf{B}_t^T \mathbf{B}_t)] \cdot v_t^2 + \frac{M}{N} [\text{tr}(\mathbf{W}_t^T \mathbf{W}_t)] \cdot \sigma^2, \end{aligned} \tag{52}$$

$$\begin{aligned} v_{t+1}^2 &= \frac{1}{N} [\|\mathbf{q}^{t+1}\|_2^2] \\ &= \mathbb{E}[\eta_t (X + \tau_t Z) - X]^2. \end{aligned} \tag{53}$$

where $X \sim P_X(x)$ is independent of $Z \sim \mathcal{N}(0, 1)$.

Even if there is no strict restriction on the distribution of singular values for general unitary invariant matrices, the performance of OAMP can still be characterized by OAMP-state evolution, which is incomparable with AMP and AMP-state evolution. Therefore, the relatively broad perception matrix makes OAMP more widely used.

The state evolution of the proposed algorithm is

$$\tau_t^2 = \frac{1}{N} [\text{tr}(\mathbf{B}_t^T \mathbf{B}_t)] + \frac{M}{N} [\text{tr}(\mathbf{W}_t^T \mathbf{W}_t)] \cdot \sigma^2, \tag{54}$$

$$v_{t+1}^2 = \frac{1}{N} \mathbb{E}[\|\mathbf{q}^{t+1}\|_2^2]. \tag{55}$$

The proposed algorithm is simplified based on the traditional OAMP algorithm, which still maintains the convergence of the OAMP algorithm. However, the convergence rate may be weaker than the traditional OAMP algorithm.

REFERENCES

- [1] I. Tomkos, D. Klondis, E. Pikasis, and S. Theodoridis, "Toward the 6G network era: Opportunities and challenges," *IT Prof.*, vol. 22, no. 1, pp. 34–38, Jan. 2020.
- [2] N. Khiadani, "Vision, requirements and challenges of sixth generation (6G) networks," in *Proc. 6th Iranian Conf. Signal Process. Intell. Syst. (ICSPIS)*, Dec. 2020, pp. 1–4.
- [3] G. Wikstrom, J. Peisa, P. Rugeland, N. Johansson, S. Parkvall, M. Girmyk, G. Mildh, and I. L. D. Silva, "Challenges and technologies for 6G," in *Proc. 2nd 6G Wireless Summit (6G SUMMIT)*, Mar. 2020, pp. 1–5.
- [4] F. Rusek and J. B. Anderson, "Constrained capacities for Faster-than-Nyquist signaling," *IEEE Trans. Inf. Theory*, vol. 55, no. 2, pp. 764–775, Feb. 2009.
- [5] J. B. Anderson, F. Rusek, and V. Öwall, "Faster-than-Nyquist signaling," *Proc. IEEE*, vol. 101, no. 8, pp. 1817–1830, Aug. 2013.
- [6] I. Darwazeh, H. Ghannam, and T. Xu, "The first 15 years of SEFDM: A brief survey," in *Proc. 11th Int. Symp. Commun. Syst., Netw. Digit. Signal Process. (CSNDSP)*, Jul. 2018, pp. 1–7.
- [7] T. Xu and I. Darwazeh, "Spectrally efficient FDM: Spectrum saving technique for 5G?" in *Proc. 1st Int. Conf. 5G Ubiquitous Connectivity*, 2014, pp. 273–278.
- [8] H. Jiang, D. Li, and W. Li, "Performance analysis of overlapped multiplexing techniques," in *Proc. 3rd Int. Workshop Signal Design Appl. Commun.*, Sep. 2007, pp. 233–237.
- [9] H. Jiang, D. Li, and W. Li, "Performance analysis of overlapped multiplexing techniques," in *Proc. 3rd Int. Workshop Signal Design Appl. Commun.*, Sep. 2007, pp. 1–6.
- [10] S. Yang and L. Hanzo, "Fifty years of MIMO detection: The road to large-scale MIMOs," *IEEE Commun. Surveys Tuts.*, vol. 17, no. 4, pp. 1941–1988, 4th Quart., 2015.
- [11] M. Yuhas, Y. Feng, and J. Bajcsy, "On the capacity of Faster-than-Nyquist MIMO transmission with CSI at the receiver," in *Proc. IEEE Globecom Workshops (GC Wkshps)*, Dec. 2015, pp. 1–6.
- [12] Z. Zhang, M. Yuksel, and H. Yanikomeroglu, "Faster-than-Nyquist signaling for MIMO communications," *IEEE Trans. Wireless Commun.*, early access, Oct. 10, 2021, doi: 10.1109/TWC.2022.3211327.
- [13] T. Xu, C. Masouros, and I. Darwazeh, "Design and prototyping of hybrid analog-digital multiuser MIMO beamforming for nonorthogonal signals," *IEEE Internet Things J.*, vol. 7, no. 3, pp. 1872–1883, Mar. 2020.
- [14] F. Rusek, "A first encounter with Faster-than-Nyquist signaling on the MIMO channel," in *Proc. IEEE Wireless Commun. Netw. Conf.*, Mar. 2007, pp. 1093–1097.
- [15] Q. Zhang, A. Liu, D. Li, X. Pan, and K. Wang, "Decoding overlapped time division multiplexing system with Fano algorithm," in *Proc. 10th Int. Conf. Wireless Commun., Netw. Mobile Comput. (WiCOM)*, 2014, pp. 284–288.
- [16] P. Lin, Y. Wang, and D. Li, "Low-complexity multiple-signal joint decoding for overlapped X domain multiplexing signalling," *IET Commun.*, vol. 12, no. 11, pp. 1273–1282, Jul. 2018.
- [17] G. Yao, H. Chen, and J. Hu, "An improved expectation propagation based detection scheme for MIMO systems," *IEEE Trans. Commun.*, vol. 69, no. 4, pp. 2163–2175, Apr. 2021.
- [18] H. Wang, A. Kosasih, C.-K. Wen, S. Jin, and W. Hardjawana, "Expectation propagation detector for extra-large scale massive MIMO," *IEEE Trans. Wireless Commun.*, vol. 19, no. 3, pp. 2036–2051, Mar. 2020.
- [19] J. Zhang, H. He, C.-K. Wen, S. Jin, and G. Y. Li, "Deep learning based on orthogonal approximate message passing for CP-free OFDM," in *Proc. IEEE Int. Conf. Acoust., Speech Signal Process. (ICASSP)*, May 2019, pp. 8414–8418.
- [20] S. Zhang, C.-K. Wen, K. Takeuchi, and S. Jin, "Deep learning based on orthogonal approximate message passing for CP-free OFDM," in *Proc. IEEE 18th Int. Workshop Signal Process. Adv. Wireless Commun. (SPAWC)*, Sapporo, Japan, May 2017, pp. 1–5.
- [21] B. Yin, M. Wu, J. R. Cavallaro, and C. Studer, "Conjugate gradient-based soft-output detection and precoding in massive MIMO systems," in *Proc. IEEE Global Commun. Conf.*, Dec. 2014, pp. 3696–3701.



YUE HU received the B.S. degree in communication engineering from Hebei Normal University, China, in 2014, and the M.S. degree in communication and information system from the North China University of Technology, Beijing, China, in 2017. He is currently pursuing the Ph.D. degree in information and communication engineering with the Beijing University of Posts and Telecommunications. His current research interests include the areas of wireless communications and networks, with an emphasis on information and coding theory.

...